ADVANCED INTELLIGENT SYSTEMS Open Access
www.advintellsyst.com

A Dual Magnetic Tunnel Junction-Based Neuromorphic Device

Jeongmin Hong, Xin Li, Nuo Xu, Hong Chen, Stefano Cabrini, Sakhrat Khizroev, Jeffrey Bokor, and Long You**

With the advent of artificial intelligence (AI) in computational devices technology, various synaptic array architectures are proposed for neuromorphic computing applications. Among them, the non-volatile memory (NVM) architectures are very promising for their small cell size, ultra-low energy consumption, and capability for large parallel data processing through 3D configurations capable of multilevel signal processing. Herein, the viability of such magnetic tunnel junction (MTJ)-based synaptic devices via fabrication and characterization of multi-junction spintronic devices is demonstrated, with the experimental results supported through micromagnetic simulations.

Dennard scaling rule, which was proposed in 1974 and had been relevant for decades due to advances in the development of metal–oxide–semiconductor field-effect transistors (MOSFETs), has finally ran out of steam.[1,2] However, the need for energy-efficient computing nowadays is even more urgent than ever before, covering numerous domains, such as large-scale sensor networks, Internet of Things (IoT), bioelectronics, and arguably, most importantly, neuromorphic computing applications.[3–18] While revisiting the reasons behind the failure of *Dennard* scaling rule, the following two major issues with the modern approach may be raised. First, the "Boltzmann limit," i.e., the statistical distribution of electrons in semiconductor energy bands sets the minimum ON/OFF switching for conventional transistors. The second is the "*von Neumann* bottleneck"; the performance of memory significantly lags behind that of the processor, which, in turn, leads to latency in conventional computer architectures.

When higher performance is expected from the existing computer infrastructure, particularly, to simulate the brain architecture in neuromorphic computers, one would 1) sacrifice the leakage of transistors, e.g., by lowering the threshold voltage of a MOSFET, and/or 2) enlarge the size of memories, such as static random-access memories (SRAMs) and embedded dynamic random-access memories (DRAMs). However, both of the approaches result in an explosive use of chip energy consumption. With the drastic increase in device counts to meet the modern systems' requirements, it is critical to consider the development of a new building block with a fundamentally different mechanism as well as delivering a unified computing-storage functionality.[3,6,19,20]

Spintronic devices have many unparalleled advantages, including data non-volatility, low operational power, radiation hardness, potential of scaling down to the sub-5 nm cell size, and natural inclination for multilevel 3D computing paradigms.[21–24] A primitive device structure for spintronics is the magnetic tunnel junction (MTJ) device, which consists of two ferromagnetic (FM) layers and a thin insulating layer (e.g., MgO) used as the tunneling barrier between the two FMs layers. Depending on the parallel (P) or anti-parallel (AP) relative orientation of the two FMs' magnetizations, the tunnel magnetoresistance (TMR) of an MTJ can be used as the read-out mechanism. As for the write mechanism, the spin-transfer torque (STT) carried by the injection current can be utilized to switch one of the FMs' magnetization, in analogy with the write process in a modern magnetization random-access memory (MRAM).[25]

Recently, significant progress has been achieved to use separate paths for write and read operations in MRAMs, for example, by inducing spin–orbit torque (SOT) or voltage-controlled magnetization anisotropy (VCMA) effects, to further lower the operation energy and improve the write endurance.[26,27]

Prof. J. Hong, X. Li, Prof. L. You
School of Optical and Electronic Information
Huazhong University of Science and Technology
Wuhan 430074, P. R. China
E-mail: jehong@berkeley.edu; lyou@hust.edu.cn

Prof. J. Hong, Dr. N. Xu, Prof. J. Bokor
Department of Electrical Engineering and Computer Sciences
University of California
Berkeley, CA 94720, USA

Prof. H. Chen
School of Materials Science and Energy Engineering
Foshan University
Foshan, Guangdong 528000, P. R. China

Dr. S. Cabrini
The Molecular Foundry
Lawrence Berkeley National Lab
Berkeley, CA 94720, USA

Prof. S. Khizroev
Department of Electrical and Computer Engineering
University of Miami
Coral Gables, FL 33146, USA

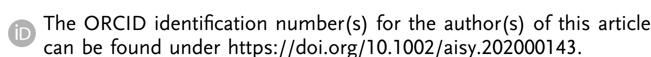
The ORCID identification number(s) for the author(s) of this article can be found under https://doi.org/10.1002/aisy.202000143.

© 2020 The Authors. Published by Wiley-VCH GmbH. This is an open access article under the terms of the Creative Commons Attribution License, which permits use, distribution and reproduction in any medium, provided the original work is properly cited.

DOI: 10.1002/aisy.202000143

26404567, 2020, 12, Downloaded from https://onlinelibrary.wiley.com/doi/10.1002/aisy.202000143 by Huazhong University Of Sci & Tech, Wiley Online Library on [02/03/2023]. See the Terms and Conditions (https://onlinelibrary.wiley.com/terms-and-conditions) on Wiley Online Library for rules of use; OA articles are governed by the applicable Creative Commons License

26404567, 2020, 12, Downloaded from https://onlinelibrary.wiley.com/doi/10.1002/aisy.202000143 by Huazhong University Of Sci & Tech, Wiley Online Library on [02/03/2023]. See the Terms and Conditions (https://onlinelibrary.wiley.com/terms-and-conditions) on Wiley Online Library for rules of use; OA articles are governed by the applicable Creative Commons License

However, despite all the progress, barely any research has been conducted to exploit the natural ability of nanomagnetic/spintronic devices to enable a new computing paradigm relying on 3D architectures capable of multilevel signal processing.[23,28] The idea of using a 3D space, instead of 2D surfaces as in the traditional devices, to store and process information is attractive not only because of the significantly increased data capacity by storing data across the thickness, but due to the capability to process information with multilevel signals.

Unlike the traditional binary information processing, multilevel signal one, with more than two signal levels, is believed to be significantly more energy efficient as well as much better suitable for realizing novel computing paradigms, such as neuromorphic computing, which is often considered the most viable next-generation alternative to the existing complementary metal oxide semiconductor (CMOS)-driven computer architecture, today.[18,29] **Figure 1**a shows a schematic of neurocomputing using electronic devices. The goal of neuromorphic computing is to realize computing with a hardware similar to that of the actual human brain. Neuromorphic computing is vital not only to simulate computationally powerful neuro-biological architectures present in the nerve system and eventually create high-performance machine learning systems, but also to improve fundamental understanding of the brain and, thus, also enable many groundbreaking medical applications.

It is not surprising that the brain does not follow the binary logic of CMOS devices. The brain logic is multilevel or even analog.[30] To study the feasibility of "multi-level per bit" capability in an MTJ structure, which is conventionally regarded as only "bi-stable" due to the uniaxial magnetization anisotropy (MA) in FM materials is worthwhile, as shown in Figure 1b. For comparison, it can be noted that the equivalent semiconductor memory option, known as the "multiple level per cell" (MLC) feature, remains subject to scaling limitations in both the planar format and the 3D configuration with vertical stacking. Furthermore, as for the rising "*Non-von Neumann*" applications, such a multilevel spintronic device is suitable for implementing synapses (weight units) in in-memory computing (e.g., hardware accelerator or spiking neural networks) systems, as shown in Figure 1c. In both situations, a magnetic "bit" will possibly become a unified storage-and-computing "byte."[18,31,32]

The proposing magnetic neuromorphic device enables a multilevel and unified storage-and-computing functionality in a single cell, which consists of non-volatile resistors. It can be tuned by applied currents or voltages and set to a large number of signal levels. The novel device utilizes a dual-domain-and-dual-domain MTJ (ddMTJ) structure to be programmed into eight weight signal levels through a spin polarized current using the STT effect. The resistive switching in our spin-torque memristor is linked to the displacement of a magnetic domain

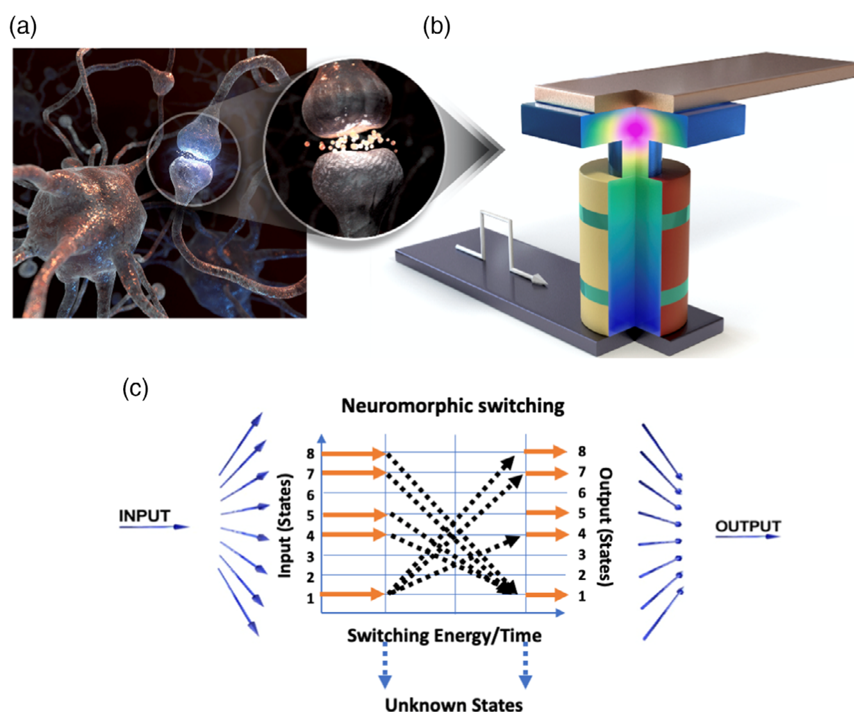

Figure 1. Descriptive schematics of neuromorphic computing using a state-of-the-art non-volatile device. a) From biological point of view, excitatory and inhibitory postsynaptic potentials are delivered from one neuron to the next through chemical and electrical messaging at synapses, driving the generation of new "action potentials." b) A detailed biological synaptic weight change could be observed to depend on the relative timing of pre- and post-synapse spikes. Neuromorphic computing signals using dual-domain and dual-junction MTJ propagate through. c) A simplified model of the synaptic weight, which can be represented by a conductance/resistance in a controlled but "blind" manner. Multiply accumulate action could be possible in an energy efficient manner. The firing initiation membrane potential threshold can be simulated by the magnetic anisotropy and coercivity of magnetic junctions. Resistance (information states) modulation by train of identical narrow pulses with fixed amplitude, potentiation, and depression will be achieved. Here, the spikes are modulated by switching energy (fixed amplitude) and pulse duration.

© 2020 The Authors. Published by Wiley-VCH GmbH

wall by spin torques in a perpendicularly magnetized MTJ. The magnetic synaptic device enables a multilevel and unified storage-and-computing functionality in a single cell. The compact cell structure as well as the high energy efficiency suggests that the proposed ddMTJ memristor is promising to serve as a primitive cell for future neuromorphic devices.

Figure 2a shows the conventional MTJ structure: there is only one tunneling barrier between two magnetic layers. Usually, the structure could have only two configurations for the relative orientations of the magnetization in the two layers, such as parallel (P) and anti-parallel (AP) states, respectively, assuming a single-domain configuration in each magnetic layer. This device can be treated as a series connection of two MTJs, each with two FMs and one barrier layer. All of the FMs act as free layers to switch their magnetization directions and contain dual magnetic domains, as shown in the right column of Figure 2a.[23] If the MTJ device's cross-sectional area is properly designed to have, not single, but multiple magnetic domains, the possible realm of configurations becomes highly non-linear and, thus, more complicated. Such multi-domain configurations are defined by an interplay between the magnetic anisotropy and spin exchange energies to minimize the net energy of the system.

For example, using ultra-high anisotropy materials, such as L_{10} phase structures, could result in domain lengths as short as 1 nm or even smaller, while maintaining the desired non-volatility of these devices.[24] Definitely, it would be hard to write and read information in such small domains independently. However, one could exploit the highly non-linear dependence of the signals if multi-domains with such short lengths are written and read back from an adequately large cell size, e.g., with a characteristic lateral size on the order of 10 nm. Figure 2b,c show that, in total, five different magnetic permutations/combinations of single and dual domains could possibly exist in a simple dual MTJ (dMTJ) with single tunnel barrier, which is labeled as states "a," "b," "c," "d," and "e," respectively. Among them, states "b," "c," and "d" are least stable, considering the inherent domain orientation due to the Oersted field.

By adding another junction to the structure and, thus, creating a dMTJ (dMTJ) device would result in magnetic configurations with four different relative orientations of the magnetization in the three layers, i.e., P/P, AP/P, P/AP, and AP/AP, respectively.[23] Figure 2d shows a schematic of dMTJ and ddMTJ structures, which consist of three FM with two barrier layers.

After stacking two dual-domain MTJs vertically, obviously, the resistance signals will have 11 different values, as shown in Figure 2e. We could select these following states, "a + a," "a + c," "a + e," "c + c," "c + d," "c + e," "d + d," and "e + e," as eight states, respectively. We neglect the cases of "a + d" and "d + e" states as two of the least stable ones, which are the least favorable demagnetization field combinations. However, again, it is important to mention that, if necessary, one can always find a material composition with an adequately high anisotropy to ensure stability of all the possible states.

To demonstrate the concept, we will work with eight signal levels to draw an equivalency to a three-binary-bit cell with eight signal levels, as shown in Figure 2f. In the case of two-domain MTJ, states "a" and "e" have the highest and lowest magnetoresistance (MR), respectively. Therefore, in a stacked ddMTJ, the states "a + a" and "e + e" will provide the highest and lowest MR, respectively. By considering the switching order of the three FMs from downward to upward saturation states, all the possible switching scenarios are listed in Figure 2e.

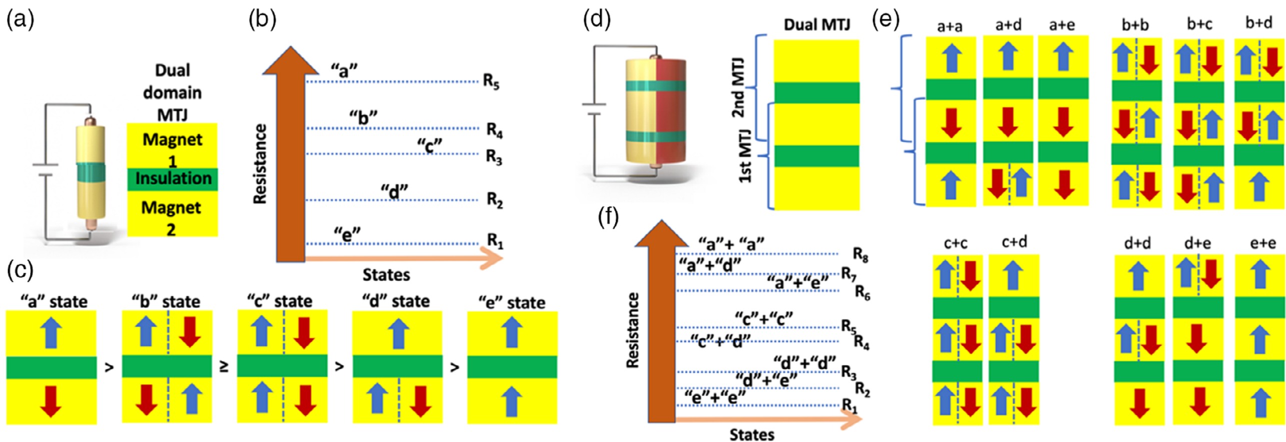

Figure 2. Schematics of the model of dual-domain MTJs (dMTJs) and dual-barrier/dual-domain MTJs (ddMTJs) and their resistance values in each ideal configuration. a) Dual-domain MTJs (ddMTJs) are shown in the left/right parts, respectively. The structures consist of two magnets with an insulation. b) The corresponding resistance values of each ideal state could be five different resistance values. c) The different resistance states could have the following configurations of the resistance. Among all of the five arrangements in the dual-domain MTJ, there are two resistance states (except for states "b," "c," and "d") in each junction structure. From the nature of domain orientation, "b," "c," and "d" states are usually ignored for the inherent domain orientation due to the Oersted field. The yellow boxes represent magnets, and the red and blue arrows show magnetization directions: either up or down. Two arrows in a yellow box denote dual-domain magnetization. d) Possible scenario of switching in ddMTJs. As the current continues to be applied, magnetization in M_1, M_2, and M_3 may change with the arrow direction. e) Depending on the orientation of each magnet, eight distinguishable resistance values could be observed. Among all of the five arrangements in the dual-domain MTJ, there are four resistance states (except for state "b") in each junction structure. From the nature of domain orientation, "b" state is ignored for the inherent domain orientation due to the Oersted field. f) Resistance values of the following states could be possible from 1 to 8. The corresponding configurations of the resistance states are shown next to the resistance values.

 © 2020 The Authors. Published by Wiley-VCH GmbH

26404567, 2020, 12, Downloaded from https://onlinelibrary.wiley.com/doi/10.1002/aisy.202000143 by Huazhong University Of Sci & Tech, Wiley Online Library on [02/03/2023]. See the Terms and Conditions (https://onlinelibrary.wiley.com/terms-and-conditions) on Wiley Online Library for rules of use; OA articles are governed by the applicable Creative Commons License

26404567, 2020, 12, Downloaded from https://onlinelibrary.wiley.com/doi/10.1002/aisy.202000143 by Huazhong University Of Sci & Tech, Wiley Online Library on [02/03/2023]. See the Terms and Conditions (https://onlinelibrary.wiley.com/terms-and-conditions) on Wiley Online Library for rules of use; OA articles are governed by the applicable Creative Commons License

The idea of adding even more layers and using spin polarized currents to write information in all the layers as well as using the giant magnetoresistance (GMR) and tunnel magnetoresistance (TMR) effect to read information back has strong merit to it. One could foresee writing and reading simultaneously hundreds or more signal levels using this 3D nanomagnetic configuration. For example, great flexibility to tailoring the magnetic anisotropy and saturation magnetization values across the thickness of such a 3D stack could be provided using the popular Co/Pt and/or Co/Pd multilayers. In these materials, the key magnetic properties are controlled by the interfacial surface as well as the thicknesses of the key elements of the composition across the thickness.[27]

As shown in **Figure 3**a, ddMTJs were fabricated to demonstrate the multi-level magnetic switching, and three FMs were deposited with the different thickness values as 0.9, 1.3, and 1.6 nm, respectively. Two MTJs were stacked in series to form the ddMTJ structure. The magnetic force microscopy (MFM) images confirm that the dual-domain structure is formed at a demagnetization state in each FM layer. Bright and dark colors show two domains in the structure. The left of Figure 3a shows the high-resolution helium ion-beam microscope (HIM) images of the structures. The diameters of the three fabricated FMs are ≈100, 110, and 120 nm, respectively. The right image of Figure 3a shows the transmission electron microscopy (TEM) image of the structure.

Figure 3b shows the *m–H* loops of the device using MOKE magnetometry. By applying magnetic field, the three FMs in the stack show distinctive magnetic properties including coercive field and saturation magnetization of ddMTJs. The detailed magnetic properties together with the fabrication process are described in the Experimental Section.

To demonstrate the concept, we will work with eight signal levels to draw an equivalency to a three-binary-bit cell with eight signal levels, as shown in Figure 3c. From the micromagnetic simulations, a current pulse is needed to switch the resistance state, whereas the current density and the pulse duration are non-unique when the current is larger than the critical current density.

Current density of the applied current required to switch the magnetization state, as well as the corresponding pulse duration. The initial states are shown in the leftmost cell of each row, and the final states are shown in the topmost cell of each column; the current density needed to switch from the initial states to the final states is shown in the crossover cell. Considering the effects of the thickness and the interfacial anisotropy energy of the three ferromagnetic layers, their effective anisotropy energy values can be selected to satisfy the inequality relationships: $K_U(M_2) < K_U(M_1) < K_U(M_3)$.

In this case, with an appropriate current density applied across the ddMTJ stack, M_2 will be switched at the smallest current value. The arrows in Figure 3c show the possible iteration from "1" to "1 − 1" in the ddMTJ stack. As shown in Figure 2e, the resistance values as the following orders: the domain structures/states are numbered according to the order of appearance:

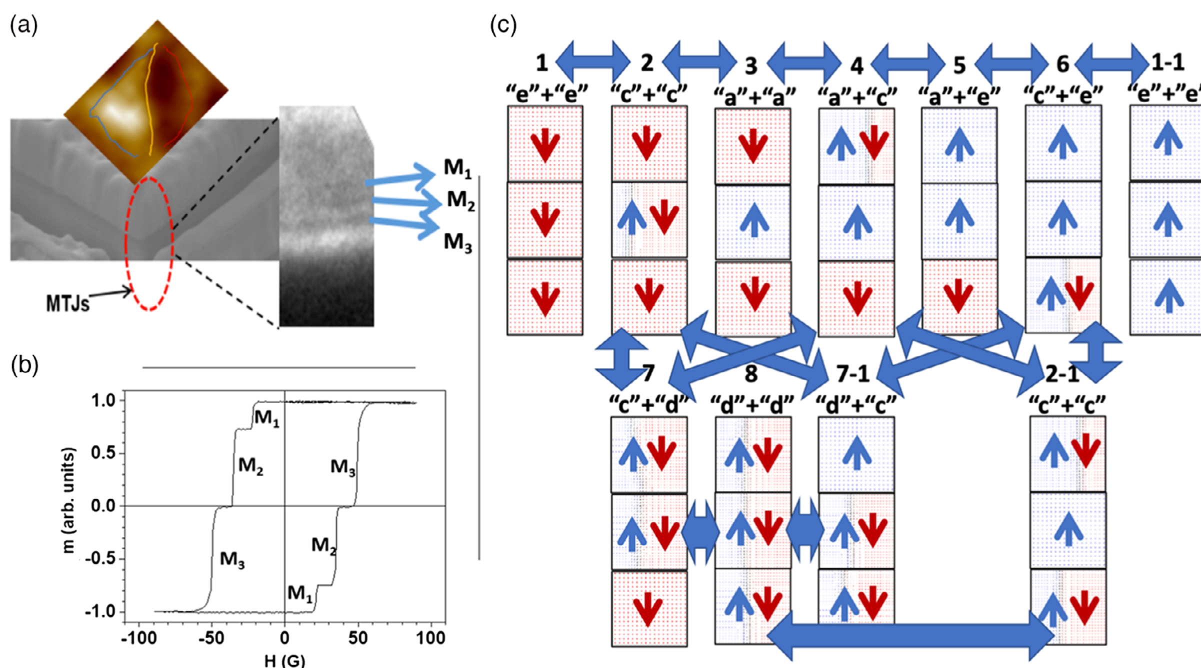

Figure 3. Magnetic properties of the dual MTJs. a) Ultra-high resolution of He-ion beam image (left) and TEM image (right) of the device stacks. An MFM image of dual-domain structures. Here, indication line shows there is only one domain wall, that is, a dual magnetic domain, at demagnetization state in the device. b) *m–H* loop of the device stacks. c) OOMMF simulation of how the signal in a dual MTJ propagates. Red arrows show that the resistance values as the following orders can be determined: the domain structures/states are numbered according to the order of the appearance: eight different resistance states "e + e," "c + c," "a + a," "a + c," "a + e," "c + e," "c + d," and "d + d" are named R_1, R_2, R_3, R_4, R_5, R_6, R_7, and R_8, respectively, for the corresponding domain structures. The numbers are based on the resistance values from the lowest to highest. Beyond that, different domain structures may correspond to one same resistance value; for example, "2" and "2 − 1" have the same resistance value of "c + c." According to the simulation results, we found that the state "d + d" is unstable between state 7 and 7 − 1, for the given values of the anisotropy energies, as described in the following.

 © 2020 The Authors. Published by Wiley-VCH GmbH

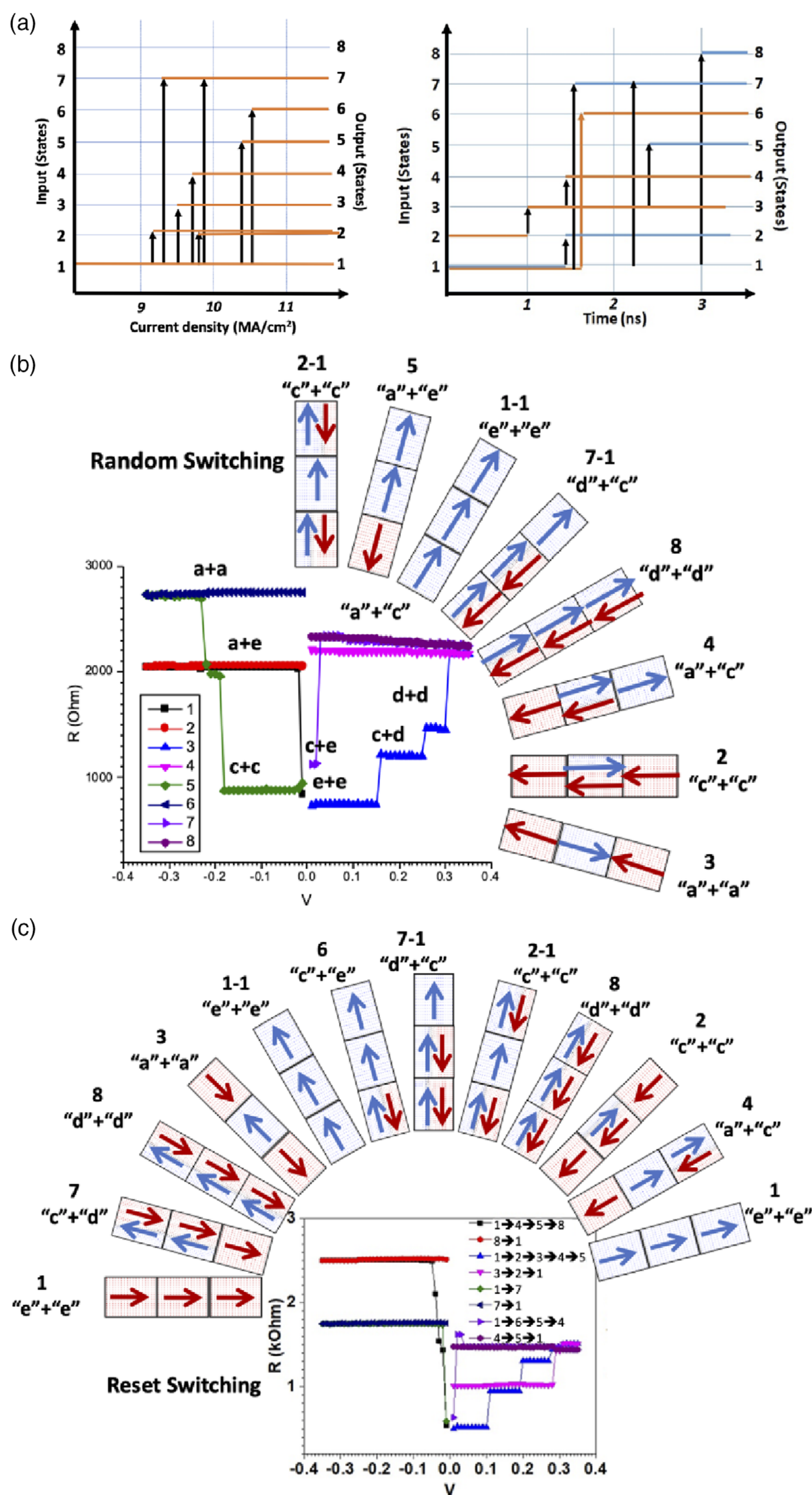

Figure 4. A scenario of the eight-level signal processing using spin computers and resulting simulation data. Resistance modulation by train of identical narrow pulses with fixed amplitude, potentiation, and depression. a) With the change of applied current pulse, the magnetization was switched in the direction of the arrows, which are consistent with the envisaged switching scenario and the resulting inputs and outputs. b) Programmable neurocomputing device and eight-level signal processing. Inset represents the signal switched from 1 to other states by varying switching energy. Random switching after demagnetization. c) Reset switching after magnetization. Resistance measurements data of reset switching.

© 2020 The Authors. Published by Wiley-VCH GmbH

26404567, 2020, 12, Downloaded from https://onlinelibrary.wiley.com/doi/10.1002/aisy.202000143 by Huazhong University Of Sci & Tech, Wiley Online Library on [02/03/2023]. See the Terms and Conditions (https://onlinelibrary.wiley.com/terms-and-conditions) on Wiley Online Library for rules of use; OA articles are governed by the applicable Creative Commons License

26404567, 2020, 12, Downloaded from https://onlinelibrary.wiley.com/doi/10.1002/aisy.202000143 by Huazhong University Of Sci & Tech, Wiley Online Library on [02/03/2023]. See the Terms and Conditions (https://onlinelibrary.wiley.com/terms-and-conditions) on Wiley Online Library for rules of use; OA articles are governed by the applicable Creative Commons License

eight different resistance states "e + e," "c + c," "a + a," "a + c," "a + e," "c + e," "c + d," and "d + d" are named R_1, R_2, R_3, R_4, R_5, R_6, R_7, and R_8, respectively, for the corresponding domain structures.

The numbers are based on the resistance values from the lowest to highest. Beyond that, different domain structures may correspond to the same resistance value; for example, "2" and "2 − 1" have the same resistance value of "c + c." According to the simulation results, we found that the state "d + d" is unstable between states 7 and 7 − 1.

For neuromorphic computing (hardware implementation of ANN), there are a number of metrics that have to be reached, for the technology or device to be useful and/or viable. One of those is the ability to tune the synaptic weight, which can be represented by a conductance/resistance in a controlled but "blind" manner. The ideal case of the device could be switched in a linear and symmetric fashion, which is critical for efficient neuromorphic computing.

As shown in **Figure 4**a, it could be programmable by the change of voltage in selected resistance states. Therefore, the proposed ddMTJ structure exhibits multiple (up to eight) resistance levels by modulating the switching values. Through the object oriented micromagnetic framework (OOMMF) simulation, current density of the applied current and the corresponding pulse duration could be determined to switch the magnetization states. Spike-timing-dependence plasticity (STDP) measurement indicated the proper values of stimulation, as shown in Supporting Information. Figure 4b presents a typical signal processing with eight distinguishable signals. By sweeping the voltage, the outputs change from the lowest to highest states, respectively. The resistance changes were observed for eight distinctive values through voltage programming, from −0.35 to 0.35 V within the range of the switching energy.

Considering the resistance and voltage programming values, the switching energy ranges from 4 to 10 MA cm^{-2}. It can be noted that R_4 and R_5 are unstable as described in the previous section. The experimental data are compared with the simulation results. The STT-multilevel device can be operational with eight different states. An input can trigger by time and switching energy together. The outputs of each magnet change followed by the switching energy up to eight resistance levels.

The initial condition of FMs in a ddMTJ was saturated to the upward state (namely "1" state). The final state with each switching energy was observed after a relaxation of 12 ns. To observe the overall switching scenario, with state "1" or "1 − 1" setting as the initial state, current should be applied from top to bottom or bottom to top of the stack, respectively, as shown in Figure 4a. From the initial state of upward saturated state, we observed that continuous pulse excitation could iterate the following scenario: it was possible to have the states one after another as the following order of the arrow, which is consistent with the aforementioned scenario, as shown in Figure 3c.

From the initial state: upward saturated state "1," any of the other seven states could be reached by applying current with a fixed duration of 0.8 ns, and among them, state "8" was an unstable state, which only appeared when the current density and the pulse duration were set as 9.0 MA cm^{-2} and 0.8 ns, respectively. Furthermore, Figure 4a shows switching between states could be achieved by applying current pulses, where the pulse duration was varying from 1 to 3 ns. A continuous pulse excitation at 0.8 ns could iterate the scenario, and it was possible to have the states one after another as the following order of the arrow.

Current density dependence from *I–V* measurements is shown in Figure 4b,c. In the case of the current applied from top to bottom in the stack, evolution of the states can only be carried on uni-directionally following the arrow direction, as shown in Figure 4b. Thus, each state can be switched to the state behind it with a current pulse applied in the case of random switching. After the reset process, the iteration shows the reset switching scenario, as shown in Figure 4c. Multiply accumulate action could be physically performed through resonance current pulses. Each state could have exactly distinguishable states through the switching energy and time. The current pulses with different switching energy could be performed to have vector-matrix multiplication.

In summary, using ddMTJ by change of time and switching energy, devices with eight signal levels were achieved. A ddMTJ device was suitable for multilevel computing, which could be fully operational using STT-ddMTJ. One of the advantages to use STT to switch the FM's magnetization is that the devices would warrant for practical applications such as a back-end-of-line (BEOL) integration scheme to the standard CMOS technology platform. The device stacks were controlled by electric fields, which could be programmable and compatible with the current CMOS technology.

Multilevel signal processing with magnetic domain-wall motion was demonstrated. The comprehensive experiments, including state-of-the-art nanofabrication and magnetotransport measurements, confirmed the feasibility and viability of the aforementioned 3D multilevel concept and were directly supported by micromagnetic simulations. The operation of MTJs clearly indicated that the device structures could also be used as 1 byte operation spin computers. In addition, the results enable a new computer paradigm for ultra-low power future spin-based neuromorphic systems.

Experimental Section

Fabrication of Dual-Barrier MTJs: Multiple CoFeB magnets and MgO insulation layers were deposited through the seven-guns sputtering system. The base pressure was as low as 1.6×10^{-8} Torr, and the process pressure range was varied between 2.0×10^{-4} and 5.0×10^{-3} Torr. The annealing temperature has been increased up to 800 K. High-quality and high-density MgO target was used for oxides layer deposition. The process pressure, gas flow, power, and deposition time have been optimized for the deposition.

Highly Sensitive Magneto-Optical Kerr (MOKE) Measurements: Ultrahigh sensitive MOKE measurement was performed using a homemade MOKE system. A 635 nm diode laser was directed toward the sample, which was located between the poles of a vector magnet. The magnetic field at the probe spot was calibrated by a three-axis Hall probe sensor (C-H3A-2 m Three Axis Magnetic Field Transducer, SENIS GmbH Zürich, Switzerland). The accuracy of the magnetic field measurement is estimated at ≈1%. The speed to sweep full hysteresis loops was 10 Oe s^{-1}.

Transport Measurements: Programmable low noise transport measurement from homemade measurement setup was performed. The sample was mounted on chip carrier after carefully wire-bonded Al wire to reduce the possible noises during the measurement. The setup guaranteed high sensitivity point contact transport measurements.

 © 2020 The Authors. Published by Wiley-VCH GmbH

OOMMF Simulation: For the device simulation, we use the publicly available OOMMF simulator to solve the LLG equation at the micromagnetics scheme.[33]

$$\frac{d\hat{m}}{dt} = -\gamma\hat{m}\times\overrightarrow{H_{\text{eff}}} + \frac{\alpha}{M_s}\hat{m}\times\frac{d\hat{m}}{dt} + \frac{-P\cdot J_e\cdot\mu_B}{e\cdot {M_s}^3}\hat{m}\times\hat{m} \times(\widehat{J_e}\cdot\nabla)\hat{m} + \frac{\xi b_J}{M_s}\hat{m}\times(\widehat{J_e}\cdot\nabla)\hat{m} \quad (1)$$

$$\text{where}\quad \overrightarrow{H_{\text{eff}}} = \frac{K_u}{M_s}\hat{z} + \frac{2A_{\text{ex}}}{{M_s}^2}\cdot\nabla^2\hat{m} - 4\pi M_s\cdot D_{zz}\cdot\hat{z}$$

In this equation, $\hat{m}$ is the normalized magnetization vector for the FM layer, γ is the gyro-magnetic ratio, α is the *Gilbert* damping constant, J_e is the current through MTJ, ξ is the ratio between *Slonczewski* and field-like torques, P is the spin polarization of the fixed layer, $\mu_B$is the *Bohr* magnetron, and e is the elementary charge. The simulation parameters are based on the size and materials from actual experiment. The saturation magnetization (M_s), exchange constant (A_{ex}), spin polarization (p), and *Gilbert* damping constant (α) values used in this work are 0.5×10^6 A m^{-1}, 30×10^{-12} J m^{-1}, 0.4, and 0.014, respectively, for the free layers. Magnetic anisotropy energy density (K_u) and thickness for the first, second, and third free layers are 1.0 MJ m^{-3} and 0.8 nm; 0.9 MJ m^{-3} and 1.2 nm; and 1.1 MJ m^{-3} and 1.6 nm. The thickness for the insulator layers is 1.2 nm. The mesh sites used in the numerical simulations are 2 nm × 2 nm × 0.4 nm.

Supporting Information

Supporting Information is available from the Wiley Online Library or from the author.

Acknowledgements

This work was supported by the National Natural Science Foundation of China under Award number 61674062. The work was also supported by the USA Department of Energy, Office of Basic Energy Sciences, and Division of Materials Sciences and Engineering under Contract No. DE-AC02-05CH11231. The work was also supported by the Office of Science, Office of Basic Energy Sciences, of the U.S. Department of Energy under Contract No. DE-AC02-05CH11231. The authors acknowledge the financial support from Air Force Office of Scientific Research (AFOSR) under Award number FA9550-18-1-0527 and the National Science Foundation (NSF) under Award numbers 0939514 (Center for Energy Efficient Electronics Sciences, E3S) and 1810270.

Conflict of Interest

The authors declare no conflict of interest.

Keywords

artificial synapses, domain walls, magnetic tunnel junction, memristors, spin-transfer torque

Received: July 1, 2020
Revised: August 31, 2020
Published online: November 4, 2020

[1] R. H. Dennard, F. Gaensslen, H.-N. Yu, L. Rideout, E. Bassous, A. LeBlanc, *IEEE J. Solid State Circuits SC–9*, **1974**.
[2] T.-J. K. Liu, K. Kuhn, *CMOS And Beyond: Logic Switches For Terascale Integrated Circuits*, 1st ed., Cambridge University, Cambridge, UK **2015**.
[3] A. W. Holger, *Protocols and Architectures for Wireless Sensor Networks*, 1st ed., John Wiley & Sons **2007**.
[4] J. Gubbi, R. Buyya, S. Marusic, M. Palaniswami, *Future Generat. Comput. Syst.* **2013**, *29*, 1645.
[5] A. Szent-Gyorgyi, *Science* **1968**, *161*, 988.
[6] J. J. Hopfield, *Proc. Natl. Acad. Sci.* **1982**, *79*, 2554.
[7] H. Lipson, M. Kurman, *Driverless: Intelligent Cars and the Road Ahead*MIT Press, Cambridge, US **2016**.
[8] M. Hu, H. Li, Y. Chen, Q. Wu, G. S. Rose, R. W. Linderman, *IEEE Trans. Neural Netw. Learn. Syst.* **2014**, *25*, 1864.
[9] S. Park, J. Noh, M.-L. Choo, A. M. Sheri, M. Chang, Y.-B. Kim, C. J. Kim, M. Jeon, B.-G. Lee, B. H. Lee, H. Hwang, *Nanotechnology* **2013**, *24*, 384009.
[10] *Springer Handbook of Computational Intelligence*, (Eds: J. Kacprzyk, W. Pedrycz), Springer, New York **2015**.
[11] G. Indiveri, B. Linares-Barranco, R. Legenstein, G. Deligeorgis, T. Prodromakis, *Nanotechnology* **2013**, *24*, 384010.
[12] F. Alibart, S. Pleutin, O. Bichler, C. Gamrat, T. Serrano-Gotarredona, B. Linares-Barranco, D. Vuillaume, *Adv. Funct. Mater.* **2012**, *22*, 609.
[13] C. D. Wright, Y. Liu, K. I. Kohary, M. M. Aziz, R. J. Hicken, *Adv. Mater.* **2011**, *23*, 3408.
[14] D. Kuzum, R. G. Jeyasingh, B. Lee, H.S. Wong, *Nano Lett.* **2012**, *12*, 2179.
[15] G. Indiveri, B. Linares-Barranco, T. J. Hamilton, A. van Shaik, R. Etienne-Cummings, T. Delbruck, S.-C. Liu, P. Dudek, P. Hafliger, S. Renaud, J. Schemmel, G. Cauwenberghs, J. Arthur, K. Hynna, F. Folowosele, S. Saighi, T. Serrano-Gotarredona, J. Wijekoon, Y. Wang, K. Boahen *Front. Neurosci.* **2011**, *5*.
[16] A. Thomas, *J. Phys. D: Appl. Phys.* **2013**, *46*, 093001.
[17] P. Krzysteczko, J. Munchenberger, M. Schafers, G. Reiss, A. Thomas, *Adv. Mater.* **2012**, *24*, 762.
[18] S. Lequeux, J. Sampaio, V. Cros, K. Yakushiji, A. Fukushima, R. Matsumoto, H. Kubota, S. Yuasa, J. Grollier, *Sci. Rep.* **2016**, *6*, 31510.
[19] J. D. Owens, M. Houston, D. Luebke, S. Green, J. E. Stone, J. C. Phillips, *Proc of the IEEE* **2008**, *96*, 879.
[20] J. V. Barth, G. Constantini, K. Kern, *Nature* **2005**, *437*, 671.
[21] J. Hong, B. Lambson, S. Dhuey, J. Bokor, *Sci. Adv.* **2016**, *2*, e1501492.
[22] J. Hong, P. Liang, V. Safonov, S. Khizroev, *J Nanopart. Res.* **2013**, *15*, 1599.
[23] J. Hong, M. Stone, B. Navarrete, K. Luongo, Q. Zheng, Z. Yuan, K. Xia, N. Xu, J. Bokor, L. You, S. Khizroev, *Appl. Phys. Lett.* **2018**, *112*, 112402.
[24] J. Hong, K. Dong, J. Bokor, L. You, *Appl. Phys. Lett.* **2018**, *113*, 062404.
[25] J.-G. Zhu, C. Park, *Mater. Today* **2006**, *9*, 36.
[26] S. Zhang, S. Luo, N. Xu, Q. Zou, M. Song, J. Yun, Q. Luo, Z. Guo, R. Li, W. Tian, X. Li, H. Zhou, H. Chen, Y. Zhang, X. Yang, W. Jiang, K. Shen, J. Hong, Z. Yuan, L. Xi, K. Xia, S. Salahuddin, B. Dieny, L. You, *Adv. Electron. Mater.* **2019**, 1800782.
[27] T. Maruyama, Y. Shiota, T. Nozaki, K. Ohta, N. Toda, M. Mizuguchi, A. A. Tulapurkar, T. Shinjo, M. Shiraishi, S. Mizukami, Y. Ando, Y. Suzuki, *Nat Nano* **2009**, *4*, 158.
[28] N. Amos, J. Butler, B. Lee, M. H. Shachar, B. Hu, Y. Tian, J. Hong, D. Garcia, R. M. Ikkawi, R. C. Haddon, D. Litvinov, S. Khizroev, *PLoS ONE* **2012**, *7*, e40134.
[29] P. Krzysteczko, J. Munchenberger, M. Schafers, G. Reiss, A. Thomas, *Adv. Mater.* **2012**, *24*, 762.

© 2020 The Authors. Published by Wiley-VCH GmbH

26404567, 2020, 12, Downloaded from https://onlinelibrary.wiley.com/doi/10.1002/aisy.202000143 by Huazhong University Of Sci & Tech, Wiley Online Library on [02/03/2023]. See the Terms and Conditions (https://onlinelibrary.wiley.com/terms-and-conditions) on Wiley Online Library for rules of use; OA articles are governed by the applicable Creative Commons License

[30] K. Seo, I. Kim, S. Jung, M. Jo, S. Park, J. Park, J. Shin, K. P. Biju, J. Kong, K. Lee, B. Lee, H. Hwang, *Nanotechnology* **2011**, *22*, 254023.
[31] S. H. Jo, T. Chang, I. Ebong, B. B. Bhadviya, P. Mazumder, W. Lu, *Nano Lett.* **2010**, *10*, 1297.
[32] L. Wang, C. Yang, J. Wen, S. Gai, Y. X. Peng, *J Mater Sci Mater Electron* **2015**, *26*, 4618.
[33] M. J. Donahue, D. G. Porter, OOMMF User's Guide, ver. 1.0 Interagency Report NISTIR 6376, National Institute of Standards and Technology, Gaithersburg, **1999**.

 © 2020 The Authors. Published by Wiley-VCH GmbH

26404567, 2020, 12, Downloaded from https://onlinelibrary.wiley.com/doi/10.1002/aisy.202000143 by Huazhong University Of Sci & Tech, Wiley Online Library on [02/03/2023]. See the Terms and Conditions (https://onlinelibrary.wiley.com/terms-and-conditions) on Wiley Online Library for rules of use; OA articles are governed by the applicable Creative Commons License